A Global Determination of Cloud Microphysics with AVHRR Remote Sensing

KAZUAKI KAWAMOTO* AND TERUYUKI NAKAJIMA

Center for Climate System Research, University of Tokyo, Tokyo, Japan

TAKASHI Y. NAKAJIMA

National Space Development Agency of Japan, Earth Observation Research Center, Tokyo, Japan

(Manuscript received 23 August 1999, in final form 7 September 2000)

ABSTRACT

An algorithm is developed for determining the cloud optical thickness and effective particle radius simultaneously on a global scale using Advanced Very High Resolution Radiometer (AVHRR) multispectral radiance data. In the algorithm, the treatment of thermal radiation in Nakajima and Nakajima is improved by reformulating the thermal emission in the atmospheric layers. At the same time, the lookup table for thermal emission is parameterized in terms of the equivalent water vapor path in order to include the effect of various vertical water vapor profiles.

The algorithm is applied to AVHRR radiance data corresponding to reported aircraft and balloon measurements of cloud microphysical parameters. A comparison shows a good agreement between in situ and satellite-retrieved values thus obtained. The algorithm is further applied to 4-month Global Area Coverage data of 1987 to generate global distributions of the cloud optical thickness and effective particle radius for every $0.5° \times 0.5°$ box in a $-60°$–$60°$ latitudinal region. Similarities and differences in the global features of the effective particle radius and the optical thickness are found as compared with the previous studies.

1. Introduction

Clouds occupy about 60% of the earth's surface area and play a considerably important role for formation of the climate through radiative and dynamical processes. For example, 1% variability of cloud amount brings a change of the earth's radiation budget by several W m^{-2} at the top of atmosphere. This value easily exceeds the radiative forcing by greenhouse gases during the past 200 yr Strabala et al. (1994) indicated the dependence of the radiation budget and climate upon cloud radiative and geometric properties. Also their large variations both in horizontal and vertical extent make situations more complex (Stowe et al. 1989).

Aerosol indirect effects on the cloud radiative forcing are another important issue for recent climate studies. Ship trail cloud phenomenon, which was first reported by Conover (1966), brought up the problem that interactions between clouds and anthropogenic pollutant may modulate noticeably the earth–atmosphere radiation budget acting as cloud condensation nuclei (CCN) (Coakley et al. 1987). Radke et al. (1989) observed the cloud microphysical structure with aircraft instruments during the First ISCCP Regional Experiment (FIRE), and found an enhanced cloud reflectivity due to a marked increase in cloud liquid water content together with a decrease in particle radius. Consistently, Albrecht (1989) pointed out that a decrease in the cloud particle radius may cause a significant increase in the cloud liquid water path through a reduction of precipitation, which will cause a reduction in washing-out effect of CCN input to the cloud system.

From the above discussion, we find it is important for evaluating the cloud effects on the earth's radiation budget to observe globally not only the macroscopic variables, such as cloud amount and height, but also the cloud optical and microphysical properties such as the cloud optical thickness and effective particle radius, which are also important parameters to control the radiation budget and dynamical processes. Motivated by this background, many researchers have performed observations of cloud microphysical properties from ground, aircraft, and satellites. Especially, two important progresses have been made since the late 1980s, that is, airborne remote sensing with radiometers having near-infrared window channels at 1.6 and 2.2 μm (Twomey

* Current affiliation: Virginia Polytechnic Institute and State University, and NASA Langley Research Center, Hampton, Virginia.

Corresponding author address: Kazuaki Kawamoto, Mail Stop 420, Atmospheric Sciences Division, NASA Langley Research Center, Hampton, VA 23681.
E-mail: k.kawamoto@larc.nasa.gov

and Cocks 1989; King et al. 1990; Rawlins and Foot 1990; Nakajima et al. 1991; Asano et al. 1995), and large-scale satellite remote sensing applied to radiances in the near-infrared windows at 3.7 μm (Arking and Childs 1985; Han et al. 1994; Platnick and Twomey 1994; Kleespies 1995; Nakajima and Nakjiama 1995; Platnick and Valero 1995; Wetzel and Stowe 1999). Those progresses have proven themselves useful for investigation of the cloud microphysical structure.

There are, however, still several important issues to accelerate popular use of the cloud microphysical remote sensing. According to Nakajima and King (1990), a 3.7-μm window channel is superior to a 2.2-μm window channel in terms of the magnitude of water refractive indices. Another advantage of using 3.7-μm channel is that we can obtain a long-term dataset of National Oceanic and Atmospheric Administration Advanced Very High Resolution Radiometer (AVHRR) channel-3 radiances. On the other hand, 3.7-μm signal contains thermal emission components from ground and cloud layers that have to be removed, since the information on the cloud optical thickness and effective particle radius is included mainly in cloud-reflected solar components in both channels. There are several methods to remove the thermal emission components. Coakley and Davies (1986) proposed a method of using nighttime data, and Kleespies (1995) utilized the viewing geometry with *GOES-7* for the cancellation of the thermal component. The method of Coakley and Davies needs a condition that the cloud microphysical properties do not change from night to day. Although Nakajima and Nakajima (1995) (hereafter referred to as NN) estimated the cloud thermal component from the inferred cloud-top temperature, their method is not suitable for global analysis for the reason described later. Wetzel and Stowe (1999) analyzed only oceanic clouds with a simplified assumption of fixed water vapor amount.

Under the circumstance that there has been no global scale analysis of cloud optical thickness and effective radius other than that of Han et al. (1994) (hereafter referred to as HRL), it will be useful to develop another analysis method from a viewpoint of independent check of the retrievals, even if both methods use identical spectral channels. For this purpose, we discuss in this paper a new algorithm for simultaneous retrievals of cloud-top temperature, optical thickness, and effective particle radius using radiances in channels 1, 3, and 4. In the following sections, we will first describe the NN's method and point out its difficulties in performing global-scale analyses and then present our new algorithm. After studying the retrieval accuracy with some numerical simulations, we will compare several satellite retrievals with in situ measured values to further validate the present algorithm. Then global analyses of cloud microphysics will be performed, which will be compared with the results of HRL.

2. Methodology

a. Nakajima and Nakajima's method and its problems

Simultaneous retrieval of the cloud optical thickness (hereafter the optical thickness is at visible wavelength) and effective particle radius is based on the fact that the radiance at a nonabsorbing visible wavelength (e.g., channel 1 of AVHRR) is mainly determined by the cloud optical thickness, while the radiance at a water-absorbing near-infrared wavelength (e.g., channel 3 of AVHRR) is mainly determined by the effective particle radius, r_e, defined as

$$r_e = \frac{\int r^3 n(r)\, dr}{\int r^2 n(r)\, dr}, \tag{1}$$

where $n(r)$ is the number size distribution at a particle radius r.

For obtaining cloud optical thickness, effective particle radius, and cloud-top temperature, simultaneously, NN use radiances in channels 1, 2, and 3 of AVHRR. Because the channel-3 radiance contains thermal radiation from the ground and the cloud layer as parts of undesirable components for determining the cloud geophysical parameters, NN tried to remove thermal components from the satellite-received radiance theoretically through the following equation,

$$\begin{aligned} L(\tau_c, r_e; \mu, \mu_0, \phi) &= L_{\text{obs}}(\tau, r_e; \mu, \mu_0, \phi) \\ &\quad - t(\tau_u, \mu)[1 - t(\tau_c, r_e; \mu) - r(\tau_c, r_e; \mu)]B(T_c) \\ &\quad - t(\tau, r_e; \mu)\frac{1 - A_g}{1 - \bar{r}(\tau, r_e)A_g}B(T_g) \\ &\quad - t(\tau, r_e; \mu)\frac{A_g}{1 - \bar{r}(\tau, r_e)A_g}t(\tau, r_e; \mu_0)\frac{\mu_0 F_0}{\pi}, \end{aligned} \tag{2}$$

where L_{obs} and L are the satellite-received signal and the solar radiance reflected by the cloud layer, respectively. Here τ, τ_u, and τ_c are the optical thicknesses of the entire atmosphere, above the cloud layer and the cloud layer itself; μ and μ_0 are the cosines of the satellite and solar zenith angles, respectively, and ϕ is the azimuthal angle of the satellite relative to the sun; A_g is the ground reflectivity, F_0 is the extraterrestrial solar flux; t is the unidirectional flux transmissivity, r_c and $\bar{r}_c$ are the unidirectional flux and spherical reflectivities of the cloud layer. Here B is the Planck function and T_c and T_g are temperatures of the cloud top and the ground surface, respectively. The cloud optical thickness and effective particle radius are then obtained from L_{obs} by an iteration method. The cloud-top brightness temperature is also retrieved with a correction of emissivity $e = 1 - t -$

r in the second term of the left-hand side of Eq. (2), which can be evaluated with the retrieved optical thickness and effective radius in each iteration step.

In the process, they adopted a lookup table (hereafter referred to as LUT) method for inversion, which is calculated assuming a model atmosphere for the observation condition. This approach has given us a serious problem for global analysis, since it is found that radiances generated with the LUTs have an unnegligible dependence of the vertical structure of the model atmosphere as shown in the next subsection.

b. Formulation of satellite-received radiances

In this subsection we reformulate the satellite-received radiances in more exact form. Let us consider the atmosphere as of a three-layer system: a layer from satellite to cloud top, cloud layer, and layer from cloud bottom to the ground. Hereafter the first and the third layer are called upper and lower layer, respectively. The cloud layer is assumed to be homogeneous loaded with the same cloud droplet size distribution and saturated water vapor with cloud-top temperature. We approximate satellite-received signals for this three-layer system with an underlying Lambert surface as follows:

For channel-1 radiance:

$$L_{\text{obs}}(\tau, r_e, Z, D; \mu, \mu_0, \phi) \cong L(\tau_c, r_e, Z, D; \mu, \mu_0, \phi) + t(\tau, r_e; \mu)\frac{A_g}{1-\overline{r_c}(\tau_c, r_e, Z, D)A_g}t(\tau, r_e; \mu_0)\frac{\mu_0 F_0}{\pi}, \quad (3)$$

where Z is the cloud-top height and D is the geometrical thickness of the cloud layer; for channel-3 radiance:

$$\begin{aligned} L_{\text{obs}}(\tau, r_e, \{w(z)\}, \{T(z)\}, D; \mu, \mu_0, \phi) \cong\ & t_u(w_{eu}; \mu)L(\tau_c, r_e, T_c, D; \mu, \mu_0, \phi)t_u(w_{eu}; \mu_0) \\ & + t_u(w_{eu}; \mu) \\ & \times [1 - t_c(\tau_c, r_e, T_c, D; \mu) - r_c(\tau_c, r_e, T_c, D; \mu)]B(T_c) \\ & + t_u(w_{eu}; \mu)t_c(\tau_c, r_e, T_c, D; \mu)t_l(w_{el}; \mu) \\ & \times \frac{1 - A_g}{1 - \overline{r_c}(\tau_c, r_e, T_c, D)A_g}B(T_g) \\ & + t_u(w_{eu}; \mu)t_c(\tau_c, r_e, T_c, D; \mu)t_l(w_{el}; \mu) \\ & \times \frac{A_g}{1 - \overline{r_c}(\tau_c, r_e, T_c, D)A_g}t_l(w_{el}; \mu_0) \\ & \times t_c(\tau_c, r_e, T_c, D; \mu_0)t_u(w_{eu}; \mu_0)\frac{\mu_0 F_0}{\pi} \\ & + f_u(w_{eu}, B(T_c); \mu) \\ & + t_u(w_{eu}; \mu)t_c(\tau_c, r_e, T_c, D; \mu)f_l(w_{el}, B(T_g); \mu), \end{aligned} \quad (4)$$

where $w(z)$ and $T(z)$ are the water vapor (g cm^{-3}) and temperature (K) vertical profiles as a function of the altitude z. Hereafter, suffixes u, c, and l stand for upper, cloud, and lower layers, respectively; w_e is the equivalent water vapor amount, which will be defined later; f is the atmospheric thermal emission. As compared with NN's algorithm, we take the contribution of atmospheric thermal emission terms into account in the present study. We neglect, however, emission from the cloud that is reflected by the surface and emission from the atmosphere above the cloud that is reflected by the cloud in (4) as in NN.

In Eq. (4), emission and transmission processes are expressed in terms of the equivalent water vapor amount w_e, which is defined as

$$w_e \int w(z)\left[\frac{P(z)}{P_g}\right]^{0.9}\left[\frac{T_g}{T(z)}\right]^{0.5} dz, \quad (5)$$

where $P(z)$ is the vertical air pressure profile as a function of altitude z; P_g is the surface pressure. These meteorological parameters can be obtained from satellite measurements or objective analysis archives as the ancillary data (hereafter referred to as AD), when we analyze actual satellite data. In this study, we use National Centers for Environmental Prediction–National Center for Atmospheric Research (NCEP–NCAR) reanalysis data as AD. To know the relationship between the equivalent water vapor amount and the unidirectional transmissivity in channel 3, we made some numerical simulations with a general radiative transfer code, RSTAR-5b, which solves the radiative transfer with a combined discrete-ordinate–matrix-operator method (Nakajima and Tanaka 1986, 1988) and LOWTRAN-7 gas absorption model (Kneizys et al. 1988). Using five model atmospheres (tropical, midlatitude summer, midlatitude winter, subarctic summer, and subarctic winter), we calculated the unidirectional transmissivity in channel 3 under the condition of changing water vapor amount with its own vertical profile fixed in each atmosphere and angle conditions. The result is shown in Fig. 1. From the figure, unidirectional transmissivity, t (i.e., t_u and t_l) in channel 3 is determined almost uniquely with the equivalent water vapor amount given in Eq. (5), even if vertical profiles of water vapor (model atmospheres) may differ. This means that the effect of the vertical water vapor profile in determining the value of transmissivity can be largely accounted for by introduction of the equivalent water vapor amount. As for thermal emissions from the atmospheric layers, they are substantially small in general, but we take them into account for a better retrieval, especially in tropical and summer subtropical regions. In addition, the contribution of the atmospheric emissions becomes larger with increasing particle radius and hence with decreasing reflected solar radiation. We calculated atmospheric thermal emission for cases in Fig. 1, and showed the result in Fig. 2 as a function of the product of the equivalent water vapor

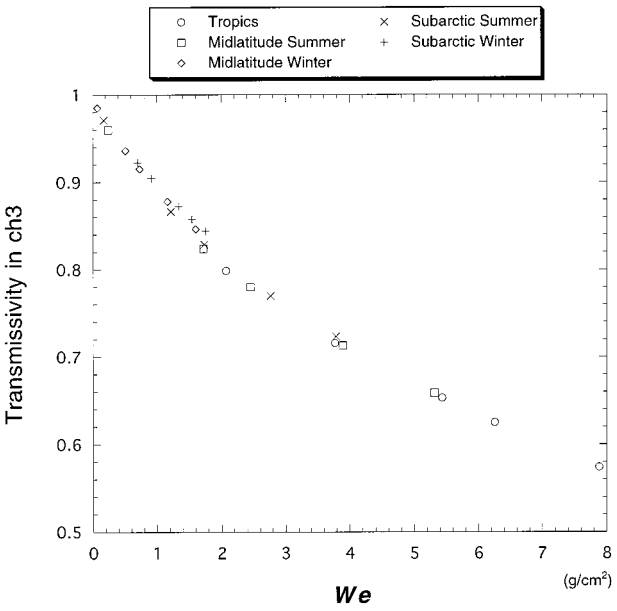

FIG. 1. Relation between transmissivity in channel 3 and the equivalent water vapor amount.

amount and Planck function, $w_e B(T)$. Here T is the temperature of the lower boundary. Figure 2 suggests a dependence similar to the $t - w_e$ relation in Fig. 1 in a sense of being determined almost uniquely with the equivalent water vapor amount, although uncertainties are increased as compared with the $t - w_e$ case due to a greater dependence on the vertical temperature profile. As for retrieving T_c, we ignore the thermal emission and the transmission in both upper and lower layers as in NN's method. Thus we approximate it simply as follows:

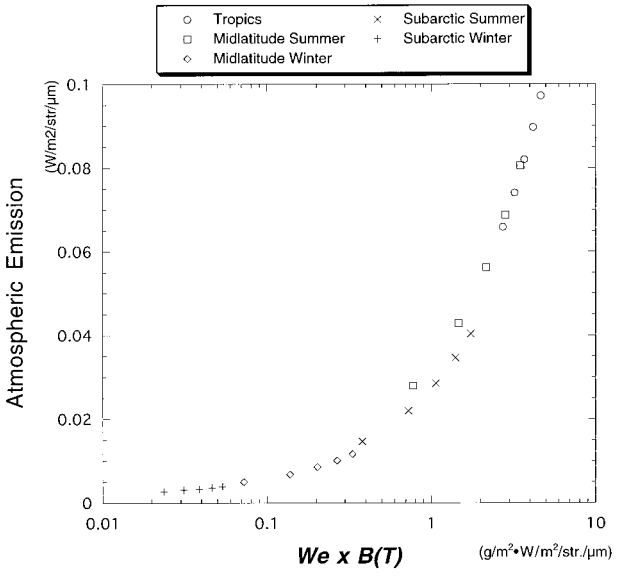

FIG. 2. Relation between atmospheric emission in channel 3 and the equivalent water vapor amount.

TABLE 1. Difference between retrieved cloud-top temperatures with Eq. (6) and input cloud-top temperatures. Here TR, MS, MW, SS, and SW are mean tropical, midlatitude summer, midlatitude winter, subarctic summer, and subarctic winter, respectively.

		TR	MS	MW	SS	SW
$\tau_c = 3$	Z = 1.5	2.65	0.73	−0.46	0.50	−0.27
	Z = 2.5	2.45	1.06	−0.38	0.82	0.49
$\tau_c = 5$	Z = 1.5	0.56	−0.40	−0.80	−0.51	−0.65
	Z = 2.5	0.06	−0.50	−0.90	−0.60	−0.44

$$T_c = B^{-1}\left[\frac{L_{\text{obs}} - t_c(\tau_c, r_e, T_c, D; \mu)(1 - A_g)B(T_g)}{1 - t_c(\tau_c, r_e, T_c, D; \mu)}\right]. \quad (6)$$

To examine this approximation, we invert T_c from simulated radiance using RSTAR-5b. The cloud optical thickness is 3 and 5, the cloud height is 1.5 and 2.5 km, and the effective particle size is 10 μm in this simulation. Differences between input and retrieved temperatures are shown in Table 1. Other than optically thin clouds in tropical atmosphere, satisfactory results are obtained in most cases. A temperature error of 2.5 K can cause r_e retrieval error of about 7%.

c. Procedure for analysis

Our procedure for inverting the cloud microphysical parameters needs several LUTs: LUT-1 for cloud-reflected solar radiances L in channels 1 and 3; LUT-2 for reflectivity r_c in channel 3, flux transmissivities t, t_c and spherical reflectivities $\bar{r}_c$ in channels 1 and 3; LUT-3 for transmissivity of the cloud layer t_c in channel 4. To construct LUTs, we used RSTAR-5b as used in the previous calculation of transmissivity and atmospheric emissions. Parameter values of the LUTs are tabulated in Table 2. To take account of subwavelength spectral characteristics of the radiometer, a wavelength averaging process is adopted as in NN.

The flow of the algorithm is shown in Fig. 3. The analysis begins with initial values assuming $\tau_c = 35$, $r_e = 15$ μm, and $Z = 2$ km, where Z is the cloud-top height. Once Z is given, T_c and the cloud-top pressure P_c are determined by the vertical temperature profile from AD. Using τ_c and P_c, the cloud type is specified through the International Satellite Cloud Climatology

TABLE 2. The grid systems of each parameter for the lookup tables.

Parameters	Grid points
Z (km)	0.5, 1.0, 1.5, 2.0, 2.5, 3.0, 4.0, 5.0, 6.0, 7.0 (channel 1)
T_c (K)	260, 270, 280, 285, 290, 295, 305 (channel 3)
D (km)	0.1, 0.2, 0.5, 1.0, 1.5, 2.0
θ (°)	0., 5., 10., 20., 30., 35., 40., 45., 50.
θ_0 (°)	0., 5., 10., 20., 30., 35., 40., 45., 50., 55., 60., 65., 70., 75.
ϕ (°)	0. ~ 180. (divided every 10°)
τ_c	1., 2., 4., 6., 9., 14., 20., 30., 50., 70.
r_e (μm)	4., 6., 9., 12., 15., 20., 25., 30.

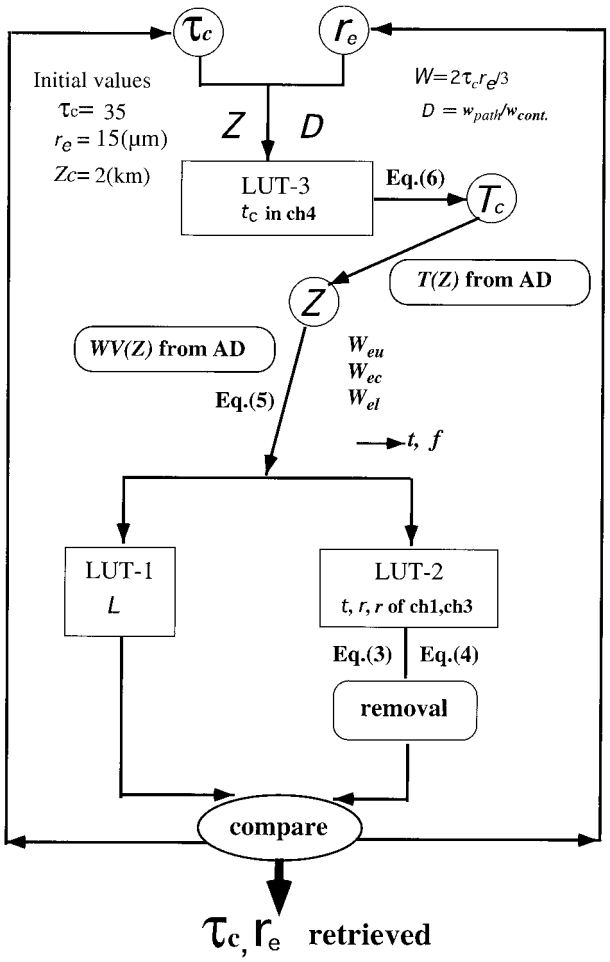

FIG. 3. Flowchart of analysis for the present algorithm.

Project (ISCCP) thresholds (Rossow et al. 1996) as shown in Fig. 4. The cloud geometrical thickness D is then obtained from $w_{\text{path}}/w_{\text{cont}}$, where w_{path} is the liquid water path and w_{cont} is the liquid water content of the cloud layer, respectively. With given τ_c and r_e, w_{path} is estimated from the relation,

$$w_{\text{path}} = \frac{2}{3}\rho\tau_c r_e, \tag{7}$$

where ρ is the density of liquid water. We assume the value of w_{cont} for each cloud type (i.e., cumulus and stratocumulus: 0.3 g m^{-3}, stratus: 0.35 g m^{-3}, altocumulus and altostratus: 0.25 g m^{-3}, and nimbostratus: 0.3 g m^{-3}) referring to Pruppacher and Klett (1978) and Heymsfield (1993). Using T_c and D, the in-cloud water vapor amount w_c is calculated with the saturation condition. Then T_c is updated using Eq. (6) with t_c from LUT-3. The renewed Z is further calculated with the updated T_c, Z, and AD. The equivalent water vapor amounts in the upper and lower layers, w_{eu} and w_{el}, are also determined simultaneously with AD. According to Eqs. (3) and (4), undesirable components are removed

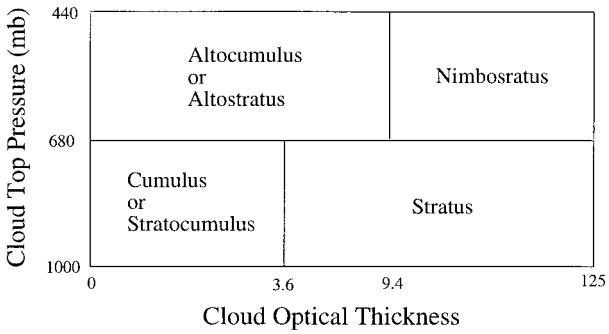

FIG. 4. ISCCP cloud-type threshold from Rossow et al. (1996). Only middle and low clouds are shown.

from observed signals L_{obs} in channels 1 and 3 by the above procedure with LUT-2 and LUT-3, and with the parameterizations of transmission and emission processes for the upper and lower layers in channel 3. Then theoretically calculated cloud-reflected radiances L in channels 1 and 3 from LUT-1 are compared with corrected L_{obs}. This comparison for determining τ_c and r_e is done alternately with fixing the other, and the calculation will be iterated until a convergence (the difference between L and corrected $L_{\text{obs}} < 0.1\%$) is achieved.

3. Validation of the present retrieval algorithm

a. Error analysis for the cloud microphysics retrieval

To evaluate the retrieval performance of our algorithm, we have applied it to simulated satellite signals calculated by RSTAR-5b with five Air Force Geophysics Laboratory (AFGL) model atmospheres. The results are shown in Fig. 5a for the cloud optical thickness and in Fig. 5b for the effective particle radius, together with the NN's results of which LUTs were constructed for the midlatitude summer model atmosphere. As for the cloud optical thickness, true values to be retrieved are 5, 10, and 15 and the effective particle radius is fixed to 10 μm for every model atmosphere. Referring to Fig. 5a, our retrievals are slightly better than NN. Actually the dependence of τ_c retrieval on model atmospheres is small for both methods, because of quite small absorption due to cloud liquid water and lack of complexity that comes from a thermal emission process unlike in channel 3. As for the effective particle radius, true values are 6, 10, and 16 μm and the cloud optical thickness is fixed to 10 for every model atmosphere. Figure 5b illustrates that our retrievals are much better than NN's and independent of model atmospheres, while NN's show a systematic dependence due to prefixed atmospheric profiles of temperature and water vapor amount. In addition to the treatment of the transmission corresponding to water vapor amount, the introduction of atmospheric thermal emissions also contributes to the better retrieval accuracy. It is also found from Figs. 5a

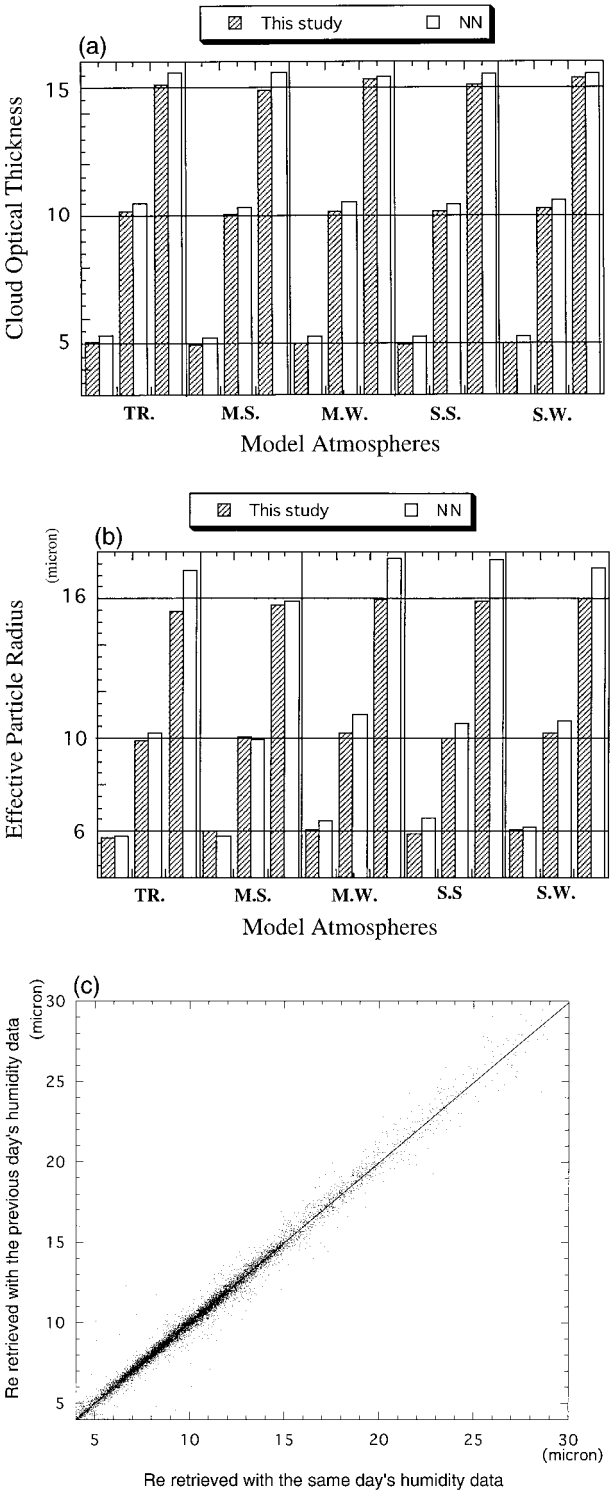

FIG. 5. (a) Comparison of the retrieval accuracy for the optical thickness between NN's method and the present algorithm. Tropical, midlatitude summer, midlatitude winter, subarctic summer, and subarctic winter model atmospheres are labeled as TR, M.S., M.W., S.S., and S.W., respectively. True values are 5, 10, and 15 from the left side, respectively. (b) As in (a) except for the effective particle radius. True values are 6, 10, and 16 μm from the left side, respectively. (c) Comparison of the retrieved particle radii with different conditions. One is with ancillary data of which the date is the same as that of satellite data, and the other is under the same condition as the previous case but for the water vapor data of 1 day before.

and 5b, the retrieval accuracy gets somewhat worse, similar to NN, as the cloud optical thickness decreases and/or the effective particle radius increases, since the relative contribution of cloud-reflected solar component gets smaller in such cases. Also as the cloud optical thickness becomes as large as 70, the retrieval accuracy gets worse, because reflected solar radiation reaches nearly the saturated value. In these cases, retrieval errors are caused by inflation of small errors such as errors due to insufficient removal of undesirable thermal emission, with formulas given by Eqs. (3), (4), (6), and (7), and wavelength averaging, especially for large solar and/or satellite zenith angles. Although we showed only one case, $Z = 2$ km, $D = 0.1$ km, $\varphi = 40$ $\varphi_o = 60°$, and $\phi = 50°$ in Figs. 5a and 5b, we have confirmed a similar accuracy of the present algorithm for other geometries.

Although we use an objective analysis dataset, it is well known that objective analysis datasets tend to have wet or dry bias. In addition to the numerical check shown in Figs. 5a and 5b, we performed the following retrieval test of the effective particle radius with different conditions for further study of the effect of water vapor amount. One is with ancillary data of which the date is the same as that of the satellite data, and the other is under the same condition as the previous case but for the water vapor data of 1 day before. Figure 5c presents the result of comparison. From this figure, we find that most of the errors caused by 1-day difference of humidity data are less than 0.5 μm, though some errors become as large as 3 μm. This analysis shows a relevance of the assumed water vapor amount and, at the same time, limitation of the method.

In our retrieval, surface reflectivity is assumed to be Lambertian, even over ocean. In order to test this assumption, we performed radiative transfer calculation with ocean surface condition using RSTAR-5b, and retrieved the cloud microphysics using the present (Lambert-assuming) algorithm. The result shows the Lambertian surface assumption could cause 6% optical thickness error and 4% droplet size error for clouds having the optical thickness 4 and effective radius 10 μm. The error rapidly decreases with increasing optical thickness.

b. Comparison with in situ measurements

In this section, we compare satellite retrievals with in situ measured values for further validation of the algorithm. For this purpose, we have surveyed airborne and balloonborne cloud microphysical measurements conducted from 1981 to 1992, and among them, we have selected cases of which location and time were close to a satellite passage we can find from our database. Table

TABLE 3. List of in situ observation information. Multiple measurements by the same author are indicated by the number.

Authors	Date	Time	Location	Surface type
Convective clouds				
Paluch° (1986) #1	11 Jul 1981	1440	47°N, 106°W	Land
#2	18 Jul 1981	1537	47°N, 106°W	Land
#3	19 Jul 1981	1625	47°N, 106°W	Land
#4	1 Aug 1981	1457	47°N, 106°W	Land
Willis et al. (1994)	11 Aug 1991	1431	28°N, 80°W	Coast
Poellot and pflaum (1989)	14 Sep 1987	1710	35°N, 98°W	Land
Gardiner and Hallett (1985)	21 Jul 1981	1440	47°N, 106°W	Land
Stratiform clouds				
Duda et al. (1991)	10 Jul 1987	0900–1830	33°N, 119°W	Ocean
Nakajima et al. (1991)	10 Jul 1987	1015	32°N, 121°W	Ocean
Meteorological Research				
Institute (1992) #1	30 Mar 1989	1130	33°N, 137°E	Ocean
#2	22 Dec 1989	1020	33°N, 142°E	Ocean
#3	14 Dec 1990	1030	32°N, 140°E	Ocean
Fric and Hoppel (1993)	18 Aug 1992	1138	45°N, 124°W	Coast

3 presents detailed information of in situ measurements involved here. In comparing these results, in situ values of the effective radius $r_{e,\text{in situ}}$ were derived from the reported droplet size distributions, while values of satellite retrievals $r_{e,\text{sat}}$ were calculated with a weight of corresponding optical thickness, in order to make both quantities equivalent, as follows:

$$r_{e,\text{sat}} = \frac{\langle \tau_c r_e \rangle}{\langle \tau_c \rangle}. \tag{8}$$

Figure 6 shows the result of the comparison. Vertical bars mean standard deviation of $r_{e,\text{sat}}$ derived from satellite measurements. It is found from the figure that the effective particle radii of both stratiform and convective clouds were retrieved successfully by the present algorithm within a satisfactory error less than 10%–15% in most cases.

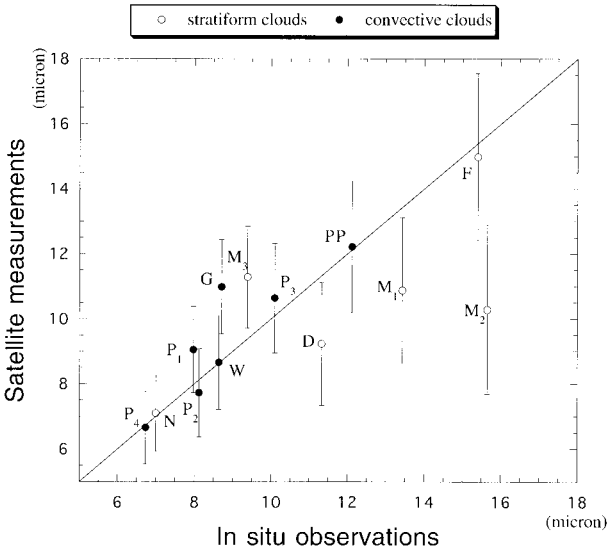

FIG. 6. Comparison of the effective particle radius obtained from in situ measurements and satellite remote sensing. Vertical bars mean standard deviation of r_e derived from satellite measurements. Here P: Paluch (1986), N: Nakajima et al. (1991), W: Willis et al. (1994), G: Gardiner and Hallett (1985), M: Meteorological Research Institute (1992), D: Duda et al. (1991), PP: Poellot and Pflaum (1989), and F: Fric and Hoppel (1993). Multiple measurements by the same authour are indicated by the number.

Previous results such as Nakajima et al. (1991) and Rawlins and Foot (1990) showed, other than King et al. (1990) which analyzed the internal radiation field, systematic overestimation of the effective particle radius as compared with corresponding in situ values, and they pointed out possible causes such as cloud anomalous absorption, imperfect calibration of the instruments, and selection of channels used. Taylor (1992) proposed an inadequacy of the gaseous absorption model (Lowtran-5) they assumed. An adoption of the updated gaseous absorption model (LOWTRAN-7) in this study may contribute to the improvement of the retrieval accuracy found here. There are many other sources of errors to cause disagreement between in situ and satellite observation, such as cirrus contamination, partial cloud cover, cloud inhomogeneity (HRL; Hayasaka et al. 1995), disagreement with the assumed size distribution (Platnick and Valero 1995), sensor discretization and calibration uncertainties (Pincus et al. 1995), slight gaps between satellite imagery and in situ measurement location temporally and spatially, uncertainties of meteorological parameters taken from AD, difference in liquid water content between the target cloud, and the classified cloud type. In our analyses, it is difficult to access all those error effects. But we found mismatch of location and time tend to bring largest uncertainty for our comparison, so that we tried to be careful to select the scene for comparison checking the reported location of the airplane on the satellite image and avoided difficult cases for the comparison due to strong cloud inhomogeneity.

The above argument clearly shows importance of conducting more validation measurements of the cloud microphysical parameters.

4. Global analyses

a. Segmentation of the satellite data and ancillary data for retrieval

In order to make an efficient global analysis, we have made global-segmented datasets of radiances for AVHRR Global Area Coverage (GAC) data. One segment box has $0.5° \times 0.5°$ spatial resolution, and there are 720×240 boxes in the analysis region of the $-60°$ to $+60°$ latitudinal belt. One hundred pixels are stored in one box with keeping $\theta < 45°$ and $\theta_0 < 70°$ to avoid imagery distortion and degradation. The segmented area is restricted within 60° in both hemispheres, since accurate retrievals are difficult to perform in high latitudes and polar regions because of large solar zenith angles and high ground reflectivities due to snow and ice. These global segmented datasets are made every day in the analysis periods.

Sensor-measured digital counts are transformed into radiances using onboard blackbody-based calibration coefficients for channels 3 and 4, and coefficients for channel 1 proposed by Kaufman and Holben (1993) because of no onboard calibration in this channel. For each box, the target cloudy pixel for the analysis is identified as a pixel corresponding to the median of the channel-1 reflectivity histogram among pixels that satisfy the conditions: channel-1 reflectivity larger than A_g, channel-4 brightness temperature smaller than $T_g - 5$ K, larger than 260 K, and standard deviation of channel-4 brightness temperatures of adjacent 2×2 pixels smaller than 4 K. The last condition was introduced in order to avoid selecting pixels of partial cloud cover and large cloud inhomogeneity (Coakley and Bretherton 1982). Although a standard deviation of 4 K can allow broken cloud cases, we adopted 4 K in order to increase the number of samples analyzed.

As for our method of analyzing only one pixel (the median of histogram) in one segment box, we make calculations to see whether it produces a representative average in the segment box or not. For this purpose, we analyzed the median of histogram, randomly selected 2, 4, and 8 pixels, and all the cloudy pixels. And then we averaged them for several segments. Figures 7a,b show the average of each selection method and the standard deviation for different segments of τ_c and r_e, respectively. It is found from the figure that one pixel sampling can be representative particularly for r_e and not cause a significant bias for τ_c, although the increased number of samplings would give better results.

Ground reflectivity A_g is assumed to be the same in one segmented box, and the smallest reflectivity out of all the values in every box for a month is adopted as A_g. While the ground surface temperature T_g and atmospheric parameters such as air temperature T, pressure P, and water vapor amount wv are obtained from NCEP–NCAR reanalysis data (AD). Values of ancillary data for each segment box are obtained by an interpolation of gridded data with $2.5° \times 2.5°$ spatial and 6-h temporal resolution.

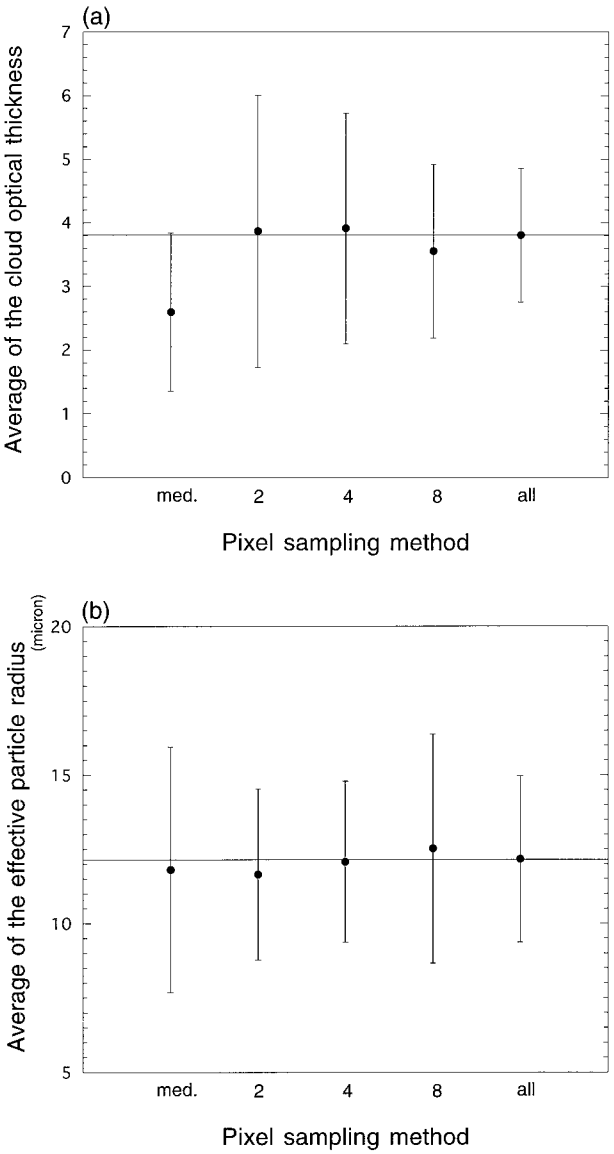

FIG. 7. (a) Averages and standard deviations of the cloud optical thickness for different pixel selection methods. A horizontal line is drawn for the average of all cloudy pixel cases. Here med.:median of the histogram, 2: randomly selected 2 pixels, 4: randomly selected 4 pixels, 8: randomly selected 8 pixels, all: all cloudy pixels. (b) As in (a) except for the effective particle radius.

b. Results and discussions

We have performed 4-month (i.e., January, April, July, and October) global analysis in 1987, which is the same period as in HRL. We made monthly composites from daily segment data, taking the average value in the boxes, which could be analyzed more than 3 times per month. Figures 8 and 9 show global monthly composites of τ_c and r_e thus obtained, respectively, for

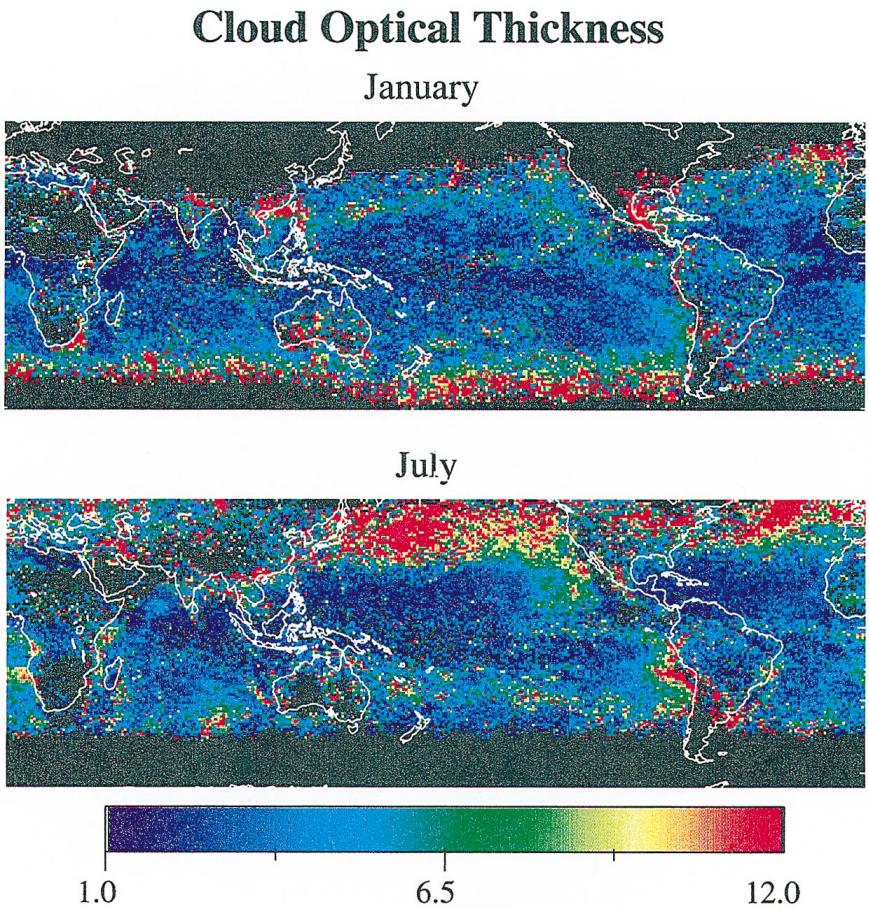

FIG. 8. Monthly mean global maps of the cloud optical thickness for clouds having $T_c > 273$ K in 1987: (top) Jan and (bottom) Jul.

clouds with $T_c > 273$ K in January and July 1987. In this work, we restrict clouds of which top temperatures are over 273 K. Limited to $\theta_0 < 70°$ to keep the retrieval accuracy, the analyzed area in the winter hemisphere is apt to be smaller than that in the summer hemisphere.

A striking characteristic of τ_c is marine stratus clouds developing extensively over the ocean around latitudes between 40° and 60° in July, although no southern counterpart appears in our result because of solar zenith angle restriction. On the other hand, it is well known that optically thick low clouds are developed by stable stratification caused by low sea surface temperature. Low stratocumulus clouds and marine fog clouds occur the regions off California and around Peru, where descendant air current of the Hadley circulation and upwelling cool ocean are dominant.

In our results, low stratocumulus and maritime fog are remarkable in July, while they decay in January. The vicissitudes of these clouds are concurrent with those of strength in ocean upwelling (Strub et al. 1987), though mechanisms of maintaining these two types of clouds may differ depending on latitudes.

Another striking phenomenon in the figure is that r_e over ocean is systematically larger than that over land, as found first by HRL. There will be two mechanisms to cause such systematic differences in the cloud microphysical structure, that is, difference in dynamics of cloud formation and difference in abundance of aerosols, which serve as CCN between ocean and land. Although we cannot conclude in this paper which is the dominant effect for making the systematic difference in the particle radius, it will be worthwhile to note two facts: 1) maritime clouds adjacent to continents such as the east coasts of China and North America and the west coast of equatorial South America and Africa have smaller droplet sizes than those of remote ocean; (2) τ_c over land is systematically larger than that over ocean, which will be seen clearly in the zonal mean values as shown in Fig. 10. Those two facts suggest the importance of two different mechanisms of the cloud enhancement due to aerosol effects as proposed by Twomey (1977) and Albrecht (1989). These phenomena can be explained by an injection of CCN-rich continental air masses due to large-scale zonal flow. In particular, this effect is remarkable in both anthropogenically and naturally polluted areas such as heavy industrial regions

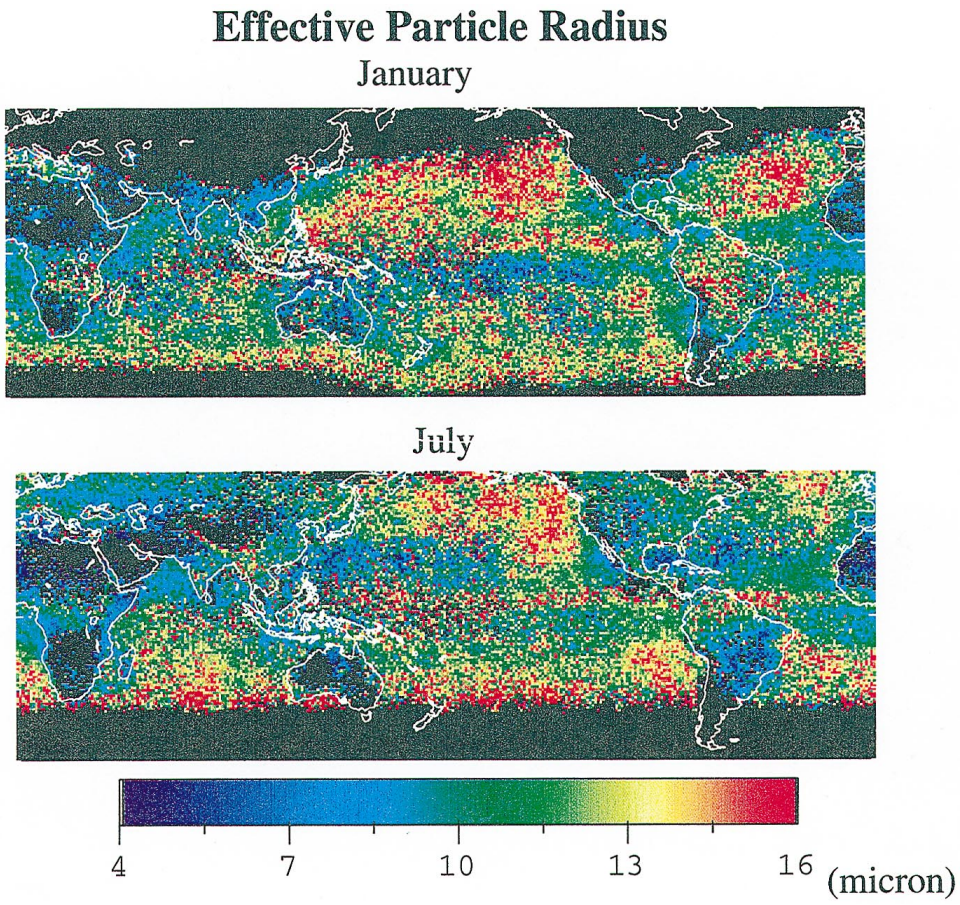

FIG. 9. As in Fig. 8 except for the effective particle radius.

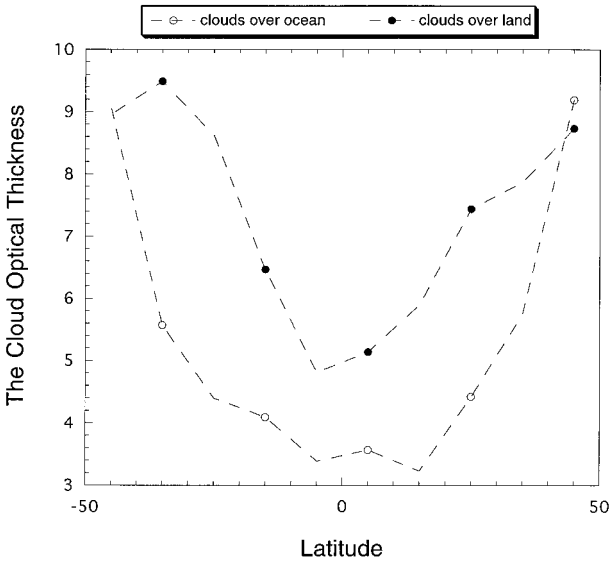

FIG. 10. Latitudinal distribution of the annual-mean optical thickness for clouds having $T_c > 273$ K.

in the northern midlatitudes and the west part of the subtropical Atlantic Ocean, which has plenty of Saharan dust particles, respectively (Husar et al. 1997; Nakajima and Higurashi 1998). These features are consistent with what have been reported by other investigators (cf. Squires 1958; Prospero et al. 1983; Han et al. 1994; Nakajima and Nakajima 1995).

Apart from the above-mentioned systematic patterns in τ_c and r_e, there are several interesting regions with large seasonal changes in those parameters suggesting dynamical effects are important. For instance, the areas having large r_e, such as over the Amazon basin and the eastern part of equatorial Africa in January would be explained by precipitation scavenging of CCN during the rainy season as suggested by HRL. This feature has been detected also in our analysis in Fig. 9 supporting this idea. Furthermore, oceanic regions having significantly small effective radii (6–8 μm) compared with the adjacent areas are found over the equatorial Pacific in January and over the western part of the northern subtropics in July. Both cases are remote oceanic regions and unlikely to be strongly influenced by anthropogenic pollutant. These optically thin clouds seem to be nonprecipitating fair weather stratocumulus of which typ-

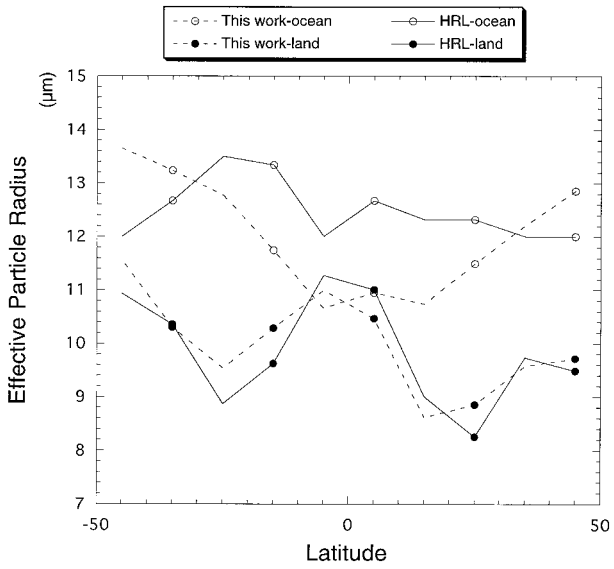

FIG. 11. As in Fig. 10 except for the effective particle radius together with the result of Han et al. (1994).

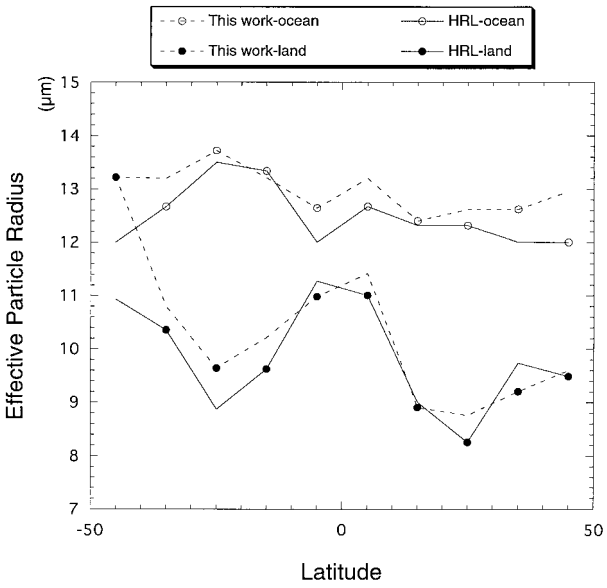

FIG. 12. As in Fig. 11 except for without the cloud-screening process.

ical value of r_e is known to be small. In fact, these shallow stratocumulus clouds are detected clearly when a cloud brokenness test by channel-4 spatial coherence is introduced in the satellite retrieval. A simple threshold method using channels 1 and 4 radiances for selecting target cloudy pixels would miss these clouds. These examples indicate that the microphysical characteristics of clouds noticeably depend on the cloud type and hence the dynamical condition of cloud formation. At the same time, this situation raises a serious question about the representativeness of cloud microphysical statistics derived with a simple cloud classification method. With a cloud brokenness test, we tend to miss cumulus type clouds from the statistics, and without the test we tend to be affected by cloud brokenness contamination in the statistics. We need an elaborate retrieval technique that can treat broken clouds suitably to remedy this problem.

Figure 10 indicates the 1987 annual- and zonal-mean latitudinal distribution of τ_c for clouds having Tc $>$ 273 K. Values over land are generally larger than those over ocean as pointed in the previous paragraphs. At the same time we find an increasing trend with latitude. Though a rapid increase over ocean would be partly due to persistent summer stratus, there are other explanations. In higher latitudes of the winter hemisphere where the solar zenith angles are large, there will be overestimation of τ_c as pointed out by Pincus et al. (1995). Davies (1984) and Loeb and Davies (1996) attributed this tendency to the so-called three-dimensional (3D) effect of clouds. A similar tendency of increasing τ_c toward higher latitudes was found by Tselioudis et al. (1992) in their study of dependence of τ_c on the cloud temperature using ISCCP data. If 3D effect is predominant in causing this feature, substantial corrections will be required in their conclusions for optical thickness versus temperature relation. In this issue, there is another discussion of overestimation of τ_c by Wang and King (1997), who suggested the importance of Rayleigh scattering effects on cloud optical thickness retrievals, especially at higher latitudes. Our results, however, will be less influenced by this effect because the LUTs in this study are made including Rayleigh scattering assuming realistic atmospheres. Here we like to notify the possibility that continental result higher than 30°N in Fig. 10 might not be representative as the annual average. Because there are few points over the continent higher than 30°N in January due mainly to snow cover as shown in Fig. 8, Fig. 10 could be weighted more on July rather than on January.

Figure 11 shows the 1987 annual- and zonal-mean latitudinal distribution of r_e for clouds having $T_c > 273$ K together with HRL's result. The zonal-mean values of r_e over ocean are larger than those over land reflecting the general characteristics shown in Fig. 9. Our values in most areas agree with HRL over land. It is interesting to find the effective particle radius is small in the Southern Hemisphere in the region between 10°S and 30°S that might be caused by biomass burning aerosols dominant in this region (Herman et al. 1997; Nakajima and Higurashi 1998). On the other hand, the discrepancy over ocean is large. This discrepancy may be explained partly by difference in cloudy pixel selection method. In particular, smaller values in the Tropics are caused by the broken cloud screening in the present algorithm as mentioned earlier (Fig. 9). We show the result without this screening in Fig 12. In this figure, our retrieval over ocean is much closer to HRL's than one in Fig. 11. In spite of such a difference, our results support the larger differences between land and ocean in the Northern

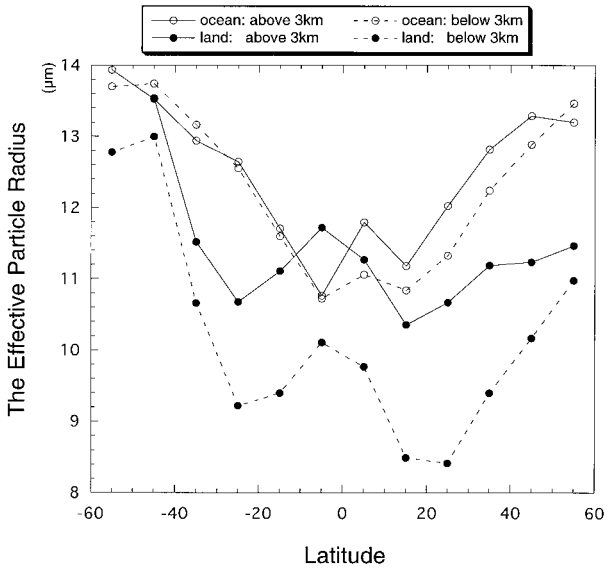

FIG. 13. Latitudinal distribution of the annual-mean effective particle radius for clouds having $T_c > 273$ K and $Z < 3$ km (lower clouds) and $Z > 3$ km (middle clouds).

Hemisphere and biomass burning region in the Southern Hemisphere as found in HRL, that can be explained by difference in natural and anthropogenic aerosol effects on the cloud droplet size.

Figure 13 shows the 1987 annual- and zonal-mean latitudinal distribution of r_e for clouds having Tc > 273 K and $Z > 3$ km (middle clouds) and $Z < 3$ km (low clouds). From this figure we notice the following points: as for clouds over land, the values of r_e for middle clouds are larger than those for low clouds; as for clouds over ocean, however, both low and middle clouds are almost the same. Moreover, we observe the difference in r_e over ocean and land decreases with cloud-top height. As pointed out similarly by HRL in their Fig. 9, these phenomena are attributed to the observed fact that aerosol number density over land decreases dramatically, while that over ocean is relatively constant with altitude as reported by Hoppel et al. (1973). Furthermore, we like to suggest a heavier aerosol burden in the Northern Hemisphere in view of larger differences of r_e between low and middle clouds both over ocean and land. These phenomena seem to be difficult, on the other hand, to be explained by dynamical processes. Global mean values of τ_c and r_e for these three kinds of clouds ($T_c > 273$ K, $Z < 3$ km, and $Z > 3$ km) over ocean and land

TABLE 4. The annual-mean values of the optical thickness for clouds having $T_c > 273$ K and $Z < 3$ km (lower clouds) and $Z > 3$ km (middle clouds), respectively, both over ocean and land.

	τ_c		
Region	$T_C > 273$ (K)	Lower clouds	Middle clouds
Ocean	5.22	5.26	6.07
Land	7.34	6.86	9.57

TABLE 5. As in Table 2 except for the effective particle radius together with the result of Han et al. (1994).

	r_e (μm)			
Region	$T_C > 273$ (K)	Han et al. (1994)	Lower clouds	Middle clouds
Ocean	11.97	11.8	12.01	12.27
Land	10.03	8.5	9.86	11.33

are listed in Tables 4 and 5, respectively, together with the HRL's results (only for r_e).

In Fig. 14, we investigate the annual-mean relationship between τ_c and r_e for clouds having $T_c > 273$ K. The knowledge of this kind of relationship is important for understanding cloud formation and decay processes of low clouds. In order to reduce a geographical mixture, we have divided the analyzed region into three parts such as midlatitude (35°–55° in latitude), subtropics (15°–35° latitude), and Tropics (lower than 15° latitude). Then we have divided the optical thickness into several bins and taken the average of the effective particle radius corresponding to each bin. According to the figure, the correlation between τ_c and r_e for maritime clouds changes from thin cloud regime (positive) to thick cloud regime (negative) at a critical optical thickness around 20–30. Similar features were reported by HRL and NN with satellite remote sensing of Californian summer stratus clouds and by Asano et al. (1995) with aircraft measurements of maritime clouds over the western Pacific Ocean. Note that this finding was made for oceanic clouds in all cases. Concerning the critical optical thickness, it is less obvious for tropical maritime clouds. This

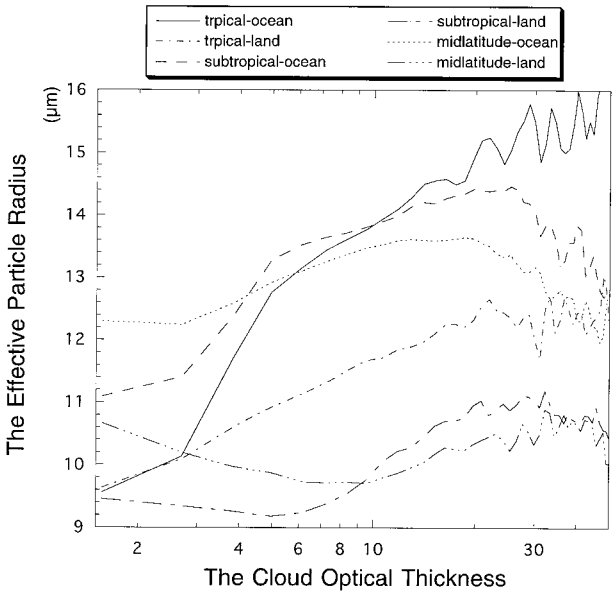

FIG. 14. The annual-mean relationship between the cloud optical thickness and effective particle radius for clouds having $T_c > 273$ K in the Tropics (lower than 15° lat), subtropics (15°–35° lat), and midlatitude (35°–55° lat).

tendency is similar to clouds over tropical land, suggesting that clouds over tropical land and ocean resemble in nature, although values of the effective radius are different by 2.5 μm. On the other hand, clouds over midlatitude land generally have a negative $\tau_c - r_e$ correlation until moderate τ_c (approximately 7–10) and a positive correlation for larger τ_c. These features may imply different mechanisms to maintain cloud processes especially for maritime and continental clouds, except Tropics where cloud characteristics are similar over land and ocean as already pointed out. In addition, over land, subtropical clouds are found to have a smaller critical optical thickness for the inversion of the correlation from negative to positive than midlatitude clouds, while over ocean, subtropical clouds are found to have a larger critical optical thickness for the inversion of the correlation than midlatitude clouds. And subtropical clouds are more variable than midlatitude clouds both over land and ocean. Baker and Charlson (1990) studied the two stable solutions for CCN abundance corresponding to clouds over ocean and land using their boundary layer model. Such stable regimes of the cloud formation depending on the CCN abundance may have the implications in the different $\tau_c - r_e$ correlations for clouds over ocean and land through aerosol–cloud interactions. Interesting areas for further research would be the relation between these characteristics and precipitation processes such as precipitation rate, precipitation efficiency, and so on.

HRL also studied the $\tau_c - r_e$ relation as discussed above, but they only divided the analyzed region into two parts as Tropics (latitude $< 30°$) and midlatitudes (latitudes between 30° and 50°) to show their tendency. With this geographical division, HRL obtained negative correlations for clouds over land, but with the critical optical thicknesses at much smaller τ_c (about 2–3). Our analysis with the same geographical division as HLR's has brought similar results other than the following two points: 1) midlatitude clouds over land have a negative correlation up to a much larger critical optical thickness of about 8, and 2) we do not find any sharp variations of r_e for small τ_c (<2). It is difficult for us to judge if point 2 is caused by difference in the retrieval algorithm or by cirrus contamination, or detecting thick aerosol hazes, as also suggested by HRL. Future validation studies of the $\tau_c - r_e$ relation are needed in order to understand the difference in cloud characteristics over ocean and land.

Table 6 shows the annual-mean values of τ_c and r_e for $T_c > 273$ K and each cloud type classified by ISCCP thresholds. In general, the values of r_e are larger for cloud types optically thicker and higher altitudes.

TABLE 6. The annual-mean values of the optical thickness and effective particle radius for cloud types classified by the ISCCP threshold method (only for $T_c > 273$ K).

	Ocean		Land	
	τ_c	r_e (μm)	τ_c	r_e (μm)
Cu or St	2.15	11.95	2.43	10.11
St	10.35	14.03	9.76	9.71
Ac or As	3.17	12.77	4.93	11.34
Nb	18.92	15.26	19.98	11.64

5. Concluding remarks

We have developed a retrieval algorithm that is capable of global-scale analysis for cloud microphysical parameters (i.e., the cloud optical thickness at visible wavelengths τ_c and effective particle radius r_e). This algorithm uses cloud-reflected solar radiances for both visible and near-infrared wavelengths based on Nakajima and Nakajima (1995). For model-atmosphere independence, we reformulated the radiances introducing an equivalent water vapor amount. Thermal emissions from the atmospheric layers are also taken into account more accurately. After checking the retrieval accuracy with numerical simulations, we further validated the present algorithm, applying it to satellite data matched up with in situ measurements. The result of comparison showed satisfactory agreement as indicated in Fig. 6.

The present algorithm was applied to 4-month AVHRR/GAC data in 1987 to produce global distributions of cloud microphysical characteristics as shown in Figs. 8 and 9. Some interesting features of cloud physical parameters with $T_c > 273$ K are found such as ocean–land contrast, near coastal regions influenced by different air masses, and seasonal variation of r_e, caused by CCN loading difference and dynamical processes. A comparison of the present results with Han et al. (1994) showed that the annual- and zonal-mean latitudinal distribution of water clouds is similar over land, but somewhat smaller over ocean. The land–ocean and height contrasts of cloud microphysical characteristics seem to support a large-scale modulation of clouds by aerosol distribution, rather than by dynamical processes.

As a further study, it will be important to investigate a diurnal variation of cloud physical field, along with the implications of other meteorological parameters. Some works have been done in view of a diurnal timescale (e.g., Minnis and Harrison 1984; Blaskovic et al. 1991). For a regional analysis of FIRE observation, Minnis et al. (1992) have used a hybrid method, which utilized the signals of both a spaceborne optical sensor and a surface-based microwave instrument, to study the diurnal behavior of stratocumulus cloud properties, and Han et al. (1995) made its validation study. More synoptic or global analyses of cloud diurnal variations, however, would bring new findings to us in the future.

Another important future study is that of cloud–aerosol interaction. In recent years, cloud properties derived from satellite data have been used for the research of aerosol–cloud interactions, or cloud modifications (e.g., Kaufman and Nakajima 1993; Platnick and Twomey 1994; Kaufman and Fraser 1997). On the other hand, Higurashi and Nakajima (1999) have recently retrieved

the aerosol optical thickness and size index over the global ocean using two channels of AVHRR. Combining their results with ours, a global view of cloud–aerosol interactions would be obtained. In addition, an analysis of long-term data of AVHRR radiances is our urgent task to understand variations of the cloud microphysical fields better, together with those of cloud–aerosol interactions in seasonal, annual, and interannual timescales.

Acknowledgments. We are grateful to J. Tucker of NASA GSFC and Ryoichi Imasu of the NIRE ARGASS (AVHRR GAC dataset for Atmosphere and Surface Studies) project for providing us with AVHRR GAC data used in this study. We thank A. Sinpo of the University of Tokyo for handling NCEP reanalysis data and S. Katagiri of CCSR for AVHRR segmented data processing. Thanks are extended to two anonymous reviewers for providing helpful suggestions. Moreover the authors are grateful to C. Twohy and R. Ruth of NCAR and the aircraft research group of the Meteorological Research Institute for supplying airborne data. The content of this paper has been submitted for the Ph.D. dissertation of K. Kawamoto to the University of Tokyo. This study was supported by NASDA OCTS/GLI projects, and the Grant-in-Aid for Scientific Research on Priority Areas (No. 08241104) of the Japanese Ministry of Education, Science, Sports and Culture.

REFERENCES

Albrecht, B. A., 1989: Aerosols, cloud microphysics and fractional cloudiness. *Science,* **245,** 1227–1230.

Arking, A., and J. D. Childs, 1985: Retrieval of cloud cover parameters from multispectral satellite measurements. *J. Climate Appl. Meteor.,* **24,** 322–333.

Asano, S., M. Shiobara, and A. Uchiyama, 1995: Estimation of cloud physical parameters from airborne solar spectral reflectance measurements for stratocumulus clouds. *J. Atmos. Sci.,* **52,** 3556–3576.

Baker, M. B., and R. J. Charlson, 1990: Bistability of CCN concentrations and thermodynamics in the cloud-topped boundary layer. *Nature,* **345,** 142–145.

Blaskovic, M., R. Davies, and J. B. Snider, 1991: Diurnal variation of marine stratocumulus over San Nicolas Island during July 1987. *Mon. Wea. Rev.,* **119,** 1469–1478.

Coakley, J. A., Jr., and F. P. Bretherton, 1982: Cloud cover from high-resolution scanner data: Detecting and allowing for partially filled fields of view. *J. Geophys. Res.,* **87,** 4917–4932.

——, and R. Davies, 1986: The effect of cloud sides on reflected solar radiation as deduced from satellite observations. *J. Atmos. Sci.,* **43,** 1025–1035.

——, R. L. Bernstein, and P. A. Durkee, 1987: Effect of ship-stack effluents on cloud reflectivity. *Science,* **237,** 1020–1022.

Conover, 1966: Anomalous cloud lines. *J. Atmos. Sci.,* **23,** 778–785.

Davies, R., 1984: Reflected solar radiances from broken cloud scenes and the interpretation of scanner measurements. *J. Geophys. Res.,* **89,** 1259–1266.

Duda, D. P., G. L. Stephens, and S. K. Cox, 1991: Microphysical and radiative profiles of marine stratocumulus from tethered balloon measurements. *J. Appl. Meteor.,* **30,** 170–186.

Fric, G. M., and W. A. Hoppel, 1993: Airship measurements of aerosol size distribution, cloud droplet spectra, and trace gas concentrations in the marine boundary layer. *Bull. Amer. Meteor. Soc.,* **74,** 2195–2202.

Gardiner, B. A., and J. Hallett, 1985: Degradation of in-cloud Forward Scattering Spectrometer Probe measurements in the presence of ice particles. *J. Atmos. Oceanic. Technol.,* **2,** 171–180.

Han, Q., W. B. Rossow, and A. A. Lacis, 1994: Near-global survey of effective droplet radii in liquid water clouds using ISCCP data. *J. Climate,* **7,** 465–497.

——, ——, R. Welch, A. White, and J. Chou, 1995: Validation of satellite retrievals of cloud microphysics and liquid water path using observation from FIRE. *J. Atmos. Sci.,* **52,** 4183–4195.

Hayasaka, T., N. Kikuchi, and M. Tanaka, 1995: Absorption of solar radiation by stratocumulus clouds: Aircraft measurements and theoretical calculations. *J. Appl. Meteor.,* **34,** 1047–1055.

Herman, J. R., P. K. Bhartia, O. Torres, C. Hsu, C. Seftor, and E. Celarier, 1997: Global distributions of UV-absorbing aerosols from Nimbus 7/TOMS data. *J. Geophys. Res.,* **102,** 16 911–16 923.

Heymsfield, A. J., 1993: Microphysical structures of stratiform and cirrus clouds. *Aerosol–Cloud–Climate Interactions,* P. V. Hobbs, Ed., Academic Press, 97–121.

Higurashi, A., and T. Nakajima, 1999: Development of a two channel aerosol retrieval algorithm on a global scale using NOAA/AVHRR. *J. Atmos. Sci.,* **56,** 924–941.

Hoppel, W. A., J. E. Dinger, and R. E. Ruskin, 1973: Vertical profiles of CCN at various geographical locations. *J. Atmos. Sci.,* **30,** 1410–1420.

Husar, R. B., J. M. Prospero, and L. L. Stowe, 1997: Characterization of tropospheric aerosols over the oceans with the NOAA Advanced Very High Resolution Radiometer optical thickness operational product. *J. Geophys. Res.,* **102,** 16 889–16 910.

Kaufman, Y. J., and B. N. Holben, 1993: Calibration of the AVHRR visible and near-IR bands by atmospheric scattering, ocean glint and desert reflection. *Int. J. Remote Sens.,* **14,** 21–52.

——, and T. Nakajima, 1993: Effect of Amazon smoke on cloud microphysics and albedo—Analysis from satellite imagery. *J. Appl. Meteor.,* **32,** 729–744.

——, and R. S. Fraser, 1997: The effect of smoke particles on clouds and climate forcing. *Science,* **277,** 1636–1639.

King, M. D., L. F. Radke, and P. V. Hobbs, 1990: Determination of the spectral absorption of solar radiation by marine stratocumulus clouds from airborne measurements within clouds. *J. Atmos. Sci.,* **47,** 894–907.

Kleespies, T. J., 1995: The retrieval of marine stratiform cloud properties from multiple observations in the 3.9-μm window under conditions of varying solar illumination. *J. Appl. Meteor.,* **34,** 1512–1524.

Kneizys, F. X., E. P. Shettle, L. W. Arbeu, J. H. Chetwynd, G. P. Anderson, W. O. Gallery, J. E. A. Selby, and S. A. Clough, 1988: Users guide to LOWTRAN-7. Air Force Geophysics Laboratory Tech. Rep. AFGL-TR-88-0177, 137 pp.

Loeb, N. G., and R. Davies, 1996: Observational evidence of plane parallel model biases: Apparent dependence of cloud optical depth on solar zenith angle. *J. Geophys. Res.,* **101,** 1621–1634.

Minnis, P., and E. F. Harrison, 1984: Diurnal variability of regional cloud and clear-sky radiative parameters derived from GOES data. Part I: Analysis method. *J. Climate Appl. Meteor.,* **23,** 993–1011.

——, P. W. Heck, D. F. Young, C. W. Fairall, and J. B. Snider, 1992: Stratocumulus cloud properties derived from simultaneous satellite and island-based instrumentation during FIRE. *J. Appl. Meteor.,* **31,** 317–339.

Meteorological Research Institute, 1992: A synthetic study on cloud-radiation processes (in Japanese). MRI Tech. Rep. 29, 340 pp.

Nakajima, T., and M. Tanaka, 1986: Matrix formulations for the transfer of solar radiation in a plane-parallel scattering atmosphere. *J. Quant. Spectrosc. Radiat. Transfer,* **35,** 13–21.

——, and M. Tanaka, 1988: Algorithms for radiative intensities calculations in moderately thick atmospheres using a truncation

approximation. *J. Quant. Spectrosc. Radiat. Transfer,* **40,** 51–69.

——, and M. D. King, 1990: Determination of the optical thickness and effective radius of clouds from reflected solar radiation measurements. Part I: Theory. *J. Atmos. Sci.,* **47,** 1878–1893.

——, and A. Higurashi, 1998: A use of two-channel radiances for an aerosol characterization from space. *Geophys. Res. Lett.,* **25,** 3815–3818.

——, M. D. King, J. D. Spinhirne, and L. F. Radke, 1991: Determination of the optical thickness and effective radius of clouds from reflected solar radiation measurements. Part II: Marine stratocumulus observations. *J. Atmos. Sci.,* **48,** 728–750.

Nakajima, T. Y., and T. Nakajima, 1995: Wide-area determination of cloud microphysical properties from NOAA AVHRR measurements for FIRE and ASTEX regions. *J. Atmos. Sci.,* **52,** 4043–4059.

Paluch, I. R., 1986: Mixing and the cloud droplet size spectrum: Generalizations from the CCOPE data. *J. Atmos. Sci.,* **43,** 1984–1993.

Pincus, R., M. Szczodrak, J. Gu, and P. Austin, 1995: Uncertainty in cloud optical depth estimates made from satellite radiance measurements. *J. Climate,* **8,** 1453–1462.

Platnick, S., and S. Twomey, 1994: Determining the susceptibility of cloud albedo to changes in droplet concentration with the Advanced Very High Resolution Radiometer. *J. Appl. Meteor.,* **33,** 334–347.

——, and F. P. J. Valero, 1995: A validation of a satellite cloud retrieval during ASTEX. *J. Atmos. Sci.,* **52,** 2985–3001.

Poellot, M. R., and J. C. Pflaum, 1989: Microphysical characteristics of convective clouds. *Atmos. Res.,* **44,** 123–136.

Prospero, J. M., R. J. Charlson, V. Mohnen, R. Jaenicke, A. C. Delany, J. Moyers, W. Zoller, and K. Rahn, 1983: The atmospheric aerosol system: An overview. *Rev. Geophys. Space. Phys.,* **21,** 1607–1629.

Pruppacher, H. R., and J. D. Klett, 1978: *Microphysics of Clouds and Precipitation.* Kluwer Academic Publishers, 954 pp.

Radke, L. F., J. A. Coakley Jr., and M. D. King, 1989: Direct and remote sensing observations of the effect of ships on clouds. *Science,* **246,** 1146–1149.

Rawlins, F., and J. S. Foot, 1990: Remotely sensed measurements of stratocumulus properties during FIRE using the C130 aircraft multichannel radiometer. *J. Atmos. Sci.,* **47,** 2488–2503.

Rossow, W. B., A. W. Walker, D. E. Beuschel, and M. D. Roiter, 1996: International Satellite Cloud Climatology Project (ISCCP) documentation of new cloud datasets. WMO/TD737, World Climate Research Programme (ICSU and WMO), 115 pp.

Squires, P., 1958: The microstructure and colloidal stability of warm clouds. Part I: The relation between structure and stability. *Tellus,* **10,** 256–261.

Stowe, L. L., H. Y. Michael, T. F. Eck, C. G. Wellemeyer, H. L. Kyle, and the *Nimbus-7* Cloud Data Processing Team, 1989: *Nimbus-7* global cloud climatology. Part II: First year results. *J. Climate,* **2,** 671–709.

Strabala, K. I., S. A. Ackerman, and W. P. Menzel, 1994: Cloud properties inferred from 8–12 mm data. *J. Appl. Meteor.,* **33,** 212–229.

Strub, P. T., J. S. Allen, A. Huyer, R. L. Smith, and R. C. Beardsley, 1987: Seasonal cycles of currents, temperatures, winds, and sea level over the northeast Pacific continental shelf: 35° to 48°. *J. Geophys. Res.,* **92,** 1507–1526.

Taylor, J. P., 1992: Sensitivity of remotely sensed effective radius of cloud droplets to changes in LOWTRAN version. *J. Atmos. Sci.,* **49,** 2564–2569.

Tselioudis, G., W. B. Rossow, and D. Rind, 1992: Global patterns of cloud optical thickness variation with temperature. *J. Climate,* **5,** 1484–1495.

Twomey, S., 1977: The influence of pollution on the shortwave albedo of clouds. *J. Atmos. Sci.,* **34,** 1149–1152.

——, and T. Cocks, 1989: Remote sensing of cloud parameters from spectral reflectance in the near-infrared. *Beitr. Phys. Atmos.,* **62,** 172–179.

Wang, M., and M. D. King, 1997: Correction of Rayleigh scattering effects in cloud optical thickness retrievals. *J. Geophys. Res.,* **102,** 25 915–25 926.

Wetzel, M. A., and L. L. Stowe, 1999: Satellite-observed patterns in stratus microphysics, aerosol optical thickness, and shortwave radiative forcing. *J. Geophys. Res.,* **104,** 31 287–31 299.

Willis, P. T., J. Hallett, R. A. Black, and W. Hendricks, 1994: An aircraft study of rapid precipitation development and electrification in a growing convective cloud. *Atmos. Res.,* **33,** 1–24.